Research Article Vol. 58, No. 26 / 10 September 2019 / Applied Optics 7073

applied optics

Measurement of rotationally symmetric aspherical surfaces with the annular subaperture stitching method

LISONG YAN,[1] DEYAN ZHU,[2] XIAOKUN WANG,[3] MING LI,[4] XUEFENG ZENG,[3] AND DONGLIN MA[1,*]

[1]School of Optical and Electronic Information, Huazhong University of Science and Technology, Wuhan 430074, China
[2]Nanjing University of Aeronautics and Astronautics, Nanjing, Jiangsu 210000, China
[3]Key Laboratory of Optical System Advanced Manufacturing Technology, Changchun Institute of Optics, Fine Mechanics and Physics, Chinese Academy of Sciences, Changchun 130033, China
[4]Intane Optics, Nanjing 210046, China
*Corresponding author: madonglin@hust.edu.cn

Received 24 June 2019; revised 1 August 2019; accepted 10 August 2019; posted 12 August 2019 (Doc. ID 370840); published 3 September 2019

The annular subaperture stitching method is an effective method for testing rotationally symmetric aspherical surfaces. To create a full aperture map of this kind of asphere, we propose an annular subaperture stitching algorithm. The algorithm is based on triangulation interpolation theory, least-square fitting method, and ray tracing method. We first show the principle of our stitching algorithm. Then, the performance of the proposed method is analyzed by simulation testing to evaluate the accuracy of the above algorithm. In the end, the experiment is given to demonstrate the correctness of our method. Both the simulation and experiment results show that the introduced method is quite effective for the testing of rotationally symmetric aspherical surfaces.

https://doi.org/10.1364/AO.58.007073

1. INTRODUCTION

Aspherical surfaces and free-form surfaces are widely used in modern optical systems because of their ability to extend the freedom of optical design, which can simplify optical construction, reduce the weight of the optical system, and correct aberrations. However, there have been problems for the manufacturing and testing of such complex surfaces, which restrict their application for long periods of time. Then, a null lens and computer-generated hologram are developed to overcome the difficulty of testing aspherical surfaces, thus promoting the wide application of aspherical surfaces [1–7]. Unfortunately, to achieve the null testing of aspherical surfaces, these kinds of auxiliary elements must be customized, and their compensating errors are hardly measured independently.

Subaperture stitching is now commonly employed to test aspherical surfaces, especially surfaces extending the aperture size limitations and slope sampling limitations of a conventional interferometer. This kind of testing was first proposed in the 1980s to overcome the limitations [8–12]. According to the subaperture shapes, circular subapertures and annular subapertures were developed separately. It is a more general method for circular subaperture testing and can be applied in not only rotationally symmetric aspherical surfaces but also in off-axis aspherical surfaces [13–17]. However, when applying the circular subaperture method to test rotationally symmetric aspherical surfaces, more subapertures are needed to cover the full aperture relative to the annular subaperture testing. Hence, the computational efficiency of a stitching algorithm, the reconstruction accuracy of the full aperture map, and the demands of a high precision hardware platform will introduce extra difficulties. In this case, annular subaperture testing is more efficient [18–22]. The number of complementary subapertures is relatively fewer, and stitching efficiency is higher.

In this paper, we focus on the iterative annular subaperture stitching algorithm and experimental demonstration of the high accuracy measurement for a rotationally symmetric aspherical surface. To evaluate the performance of the above stitching algorithm, it has been applied for the simulation testing and a 250 mm rotationally symmetric aspherical surface testing experiment. The paper is organized as follows. In Section 2, the basic theory of an annular subaperture stitching algorithm is introduced. In Section 3, the effectiveness of our method is shown by simulation. In Section 4, we demonstrate the performance of our stitching algorithm by testing a 250 mm rotationally symmetric aspherical surface. Finally, the conclusion is given in Section 5.

1559-128X/19/267073-07 Journal © 2019 Optical Society of America

2. THEORY

A. Non-Null Testing Errors for Annular Subapertures

Consider that annular subaperture testing is efficient in the measurement for a rotationally symmetric aspherical surface. The sketch map of the testing setup is shown in Fig. 1.

In the measurement, the aspheric surface is moved gradually away from the interferometer to make the reference spherical surface match the corresponding annular subaperture zone. Thus, in the zone areas, the fringes can be resolved by the charge-coupled Device (CCD). As in the annular subaperture testing, a standard spherical surface is treated as the reference surface to test the annular area of the aspherical surface; further, the testing rays will follow different paths from the reference rays, which introduce extra aberrations in the interferogram. These kinds of non-null testing errors can be calculated with the ray tracing method; in addition, it should be removed before stitching, as it's not a manufactory surface error but an extra aberration due to the non-null testing.

An interferogram in annular subaperture testing includes not only the surface error of the testing aspheric surface but also the non-null testing error, alignment error, and retrace coordinate error [23]. The relative wavefront obtained can be expressed as follows:

$$W_{\text{interferometer}} = W_{\text{non-null}} \oplus W_{\text{alignment}} \oplus W_{\text{coordinate}} \oplus W_{\text{test}}, \tag{1}$$

where $W_{\text{interferometer}}$ is the measured wavefront, $W_{\text{non-null}}$ is the non-null testing error of the annular subaperture, $W_{\text{alignment}}$ is the alignment error between interferometer and the testing annular subaperture, $W_{\text{coordinate}}$ is the non-null testing coordinate error, and W_{test} is the surface error of the annular subaperture. Note that "$\oplus$ " in Eq. (1) denotes the variables not simply added up. Thus, the testing map of interferometer $W_{\text{interferometer}}$ depends on the non-null testing error, the alignment error, the non-null testing, and the surface error of the annular subaperture.

According to the designed optical testing path, the non-null testing error can be calculated with the ray tracing method. The relative wavefront aberration is obtained by tracing rays to the exit pupil of the interferometer. If the parameters of the internal optics in the interferometer are known, we can continue to trace rays to the image plane of the interferometer. For the central subaperture, which is a rotational symmetric circular subaperture, the non-null testing error behaves like a combination of power and spherical aberrations, as shown in Fig. 2. For the other annular subapertures, the behavior of the non-null testing errors is shown in Fig. 3.

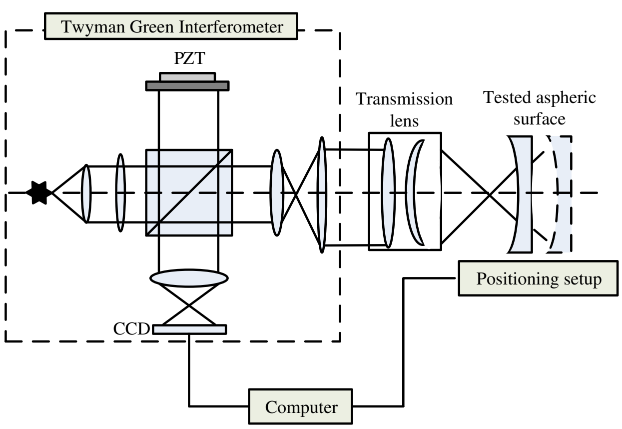

Fig. 1. Sketch map of testing setup.

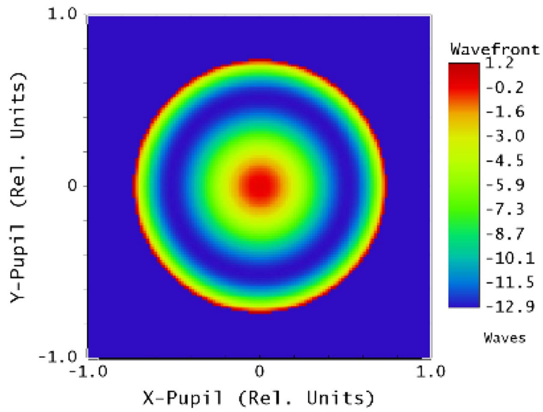

Fig. 2. Non-null testing error for central subaperture.

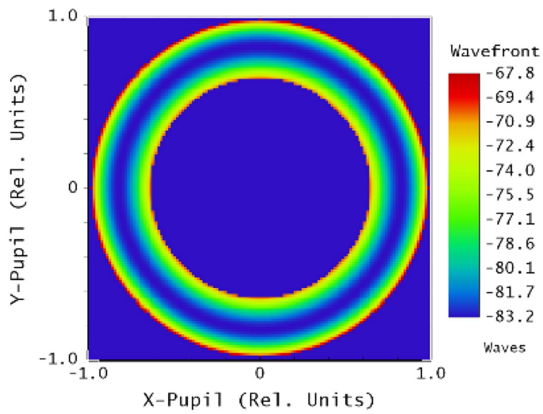

Fig. 3. Non-null error for annular subapertures.

After acquiring the non-null testing errors, the non-null testing error and the non-null testing coordinate error can be removed from the subaperture testing map at the same time. The alignment errors between subapertures can be separated with the triangulation interpolation stitching algorithm for the annular subapertures introduced in Section 2.B.

B. Triangulation Interpolation Stitching Algorithm for Annular Subapertures

The whole aspherical surface map reconstruction process of our triangulation interpolation stitching algorithm for annular subapertures is illustrated in Fig. 4.

Before stitching, the non-null testing errors of subapertures should be removed from annular subaperture maps, and all the coordinates of each subaperture should be unified in a global coordinate at this time.

The coordinates' relationship between adjacent annular subapertures is shown in Fig. 5. There is an overlapping area between adjacent subapertures, and the relative overlapping

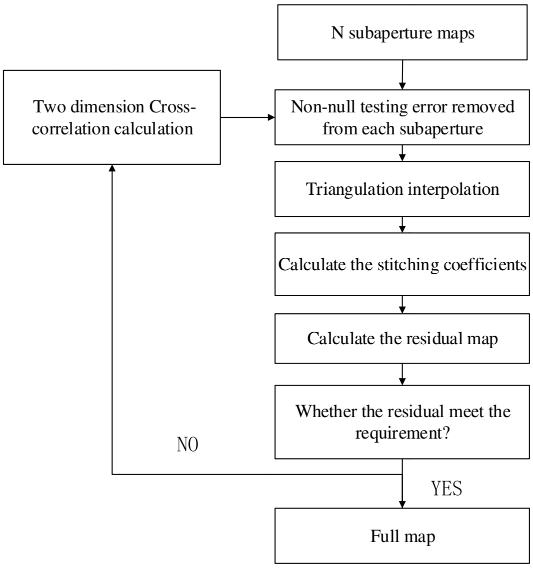

Fig. 4. Flow chart of annular subapertures stitching.

correspondence should be found in advance to calculate the stitching coefficients of each subaperture. To accomplish this work, grid points, which represent the same points between subapertures, should be defined.

A uniform grid is defined on the X-Y plane, as shown in Fig. 5. For the sake of brevity, only the grid points in the overlapping area are displayed in Fig. 5. The coordinates of the grid points in the z direction can be calculated in their respective subapertures.

Considering the grid points in the overlapping area, the testing points are displayed as "×", and the triangle is the Delaunay triangulation result to the phase data of the ith subaperture, as shown in Fig. 6.

The plane equation of each triangle can be described by Eq. (2):

$$\begin{pmatrix} x_1 & y_1 & 1 \\ x_2 & y_2 & 1 \\ x_3 & y_3 & 1 \end{pmatrix} \begin{pmatrix} a \\ b \\ d \end{pmatrix} = \begin{pmatrix} -z_1 \\ -z_2 \\ -z_3 \end{pmatrix}, \tag{2}$$

where (x_1, y_1, z_1), (x_2, y_2, z_2), and (x_3, y_3, z_3) are the coordinates of the three points making up the triangle. a, b, and d are plane coefficients to be solved of the equation

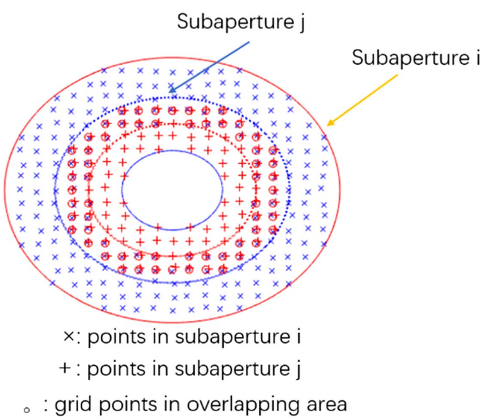

Fig. 5. Annular subaperture projection on the X-Y plane.

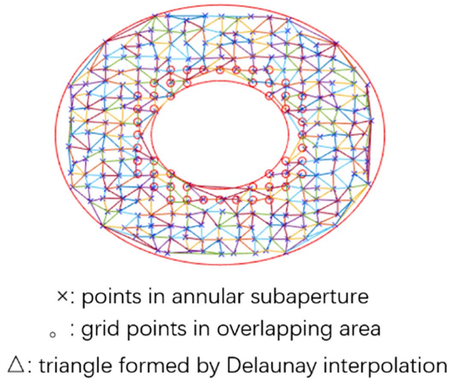

Fig. 6. Triangulation interpolation for annular subaperture.

$$z = -ax - by - d, \tag{3}$$

which is used to describe the plane equation of the triangle.

As the grid points in the overlapping area will fall into a triangle obtained with Delaunay triangulation, the coordinates in the z direction of grid points in each annular subaperture can be acquired by Eqs. (2) and (3).

After obtaining the coordinates of grid points in the z direction in each subaperture, stitching coefficients should be calculated in order to remove the alignment errors between subapertures, as described in the following.

For convenience, we assume that there are N subapertures, and the Nth subaperture is taken as a standard; then, the phase map of the ith subaperture can be expressed as

$$Z_i'(x, y) = Z_i(x, y) + \sum_{j=1}^{L} a_{ij} f_j(x, y), \tag{4}$$

where $Z_i(x, y)$ is the testing map of the ith annular subaperture, and $f_j(x, y)$ is the misalignment error functions for annular subaperture, while a_{ij} is the relative stitching coefficient to be fitted.

Applying the least-square method to Eq. (4),

$$\min = \sum_{i=1\ldots N} \sum_{\substack{k=1\ldots N \\ k\neq i}}^{i\cap k} \left[\left(Z_i(x, y) + \sum_{j=1}^{L} a_{ij} f_j(x, y) \right) - \left(Z_k(x, y) + \sum_{j=1}^{L} a_{kj} f_j(x, y) \right) \right]^2. \tag{5}$$

A group of linear equations can be transformed from Eq. (5), as shown in Eq. (6):

$$P = Q \cdot R, \tag{6}$$

where P, Q, and R are defined as follows:

1. P is a vector in length of $(N-1) \times L$ row, and the element in it can be expressed as

$$P_{(M-1) \cdot j} = \sum_{M-1} \sum_{\substack{i=1 \\ i\neq(M-1)}}^{N} f_j(x, y)(Z_{(M-1)}(x, y) - Z_i(x, y)) c_{i(M-1)}, \tag{7}$$

where $P_{(M-1)\cdot j}$ is the $((M-1)\cdot L+j)$th row of the vector P and

$$c_{ij}=\begin{cases}1 & i\cap j\neq\varnothing\\ 0 & i\cap j=\varnothing\end{cases}. \tag{8}$$

2. Q is a matrix in size of $(N-1)\times L$, and the element in it can be expressed as

$$Q_{((M-1)\cdot j)((H-1)\cdot k)}=\begin{cases}-\sum\limits_{(M-1)}\sum_{i=1,\, i\neq(M-1)}^{N} f_j(x,y)\cdot f_k(x,y)\cdot c_{i(M-1)} & M=H\\ \sum\limits_{M-1}\sum\limits_{H-1} f_j(x,y)\cdot f_k(x,y)\cdot c_{(M-1)(H-1)} & M\neq H\end{cases}, \tag{9}$$

where $Q_{((M-1)\cdot j)((H-1)\cdot k)}$ is the element of row $((M-1)\cdot L+j)$, column $((H-1)\cdot L+k)$ in the matrix Q.

3. R is a vector n length of $(N-1)\times L$ row, and the element in it can be expressed as

$$R_{(M-1)\cdot j}=a_{(M-1)j}, \tag{10}$$

where $R_{(M-1)\cdot j}$ is the element of the row $((M-1)\cdot L+j)$ in the vector R.

Stitching coefficients can be obtained by Eqs. (6)–(10), and the alignment errors can be removed from each annular subaperture. After combining subapertures together, the full aperture map is acquired [24].

3. SIMULATION

We carried out a simulation to demonstrate the effectiveness of our proposed method. For a rotationally symmetric hyperboloid surface whose conic constant k is −1.03, the diameter is 250 mm, and the vertex radius of the convex mirror is about 513.6 mm, the departure between the above aspheric surface and the best-fit sphere is shown in Fig. 7.

In the simulation, four annular subapertures are tested. Their positions and departures are shown in Fig. 8. Overlapping areas exist between every adjacent subaperture.

The original map of the tested surface within the diameter region of 28 to 80 mm is shown in Fig. 9.

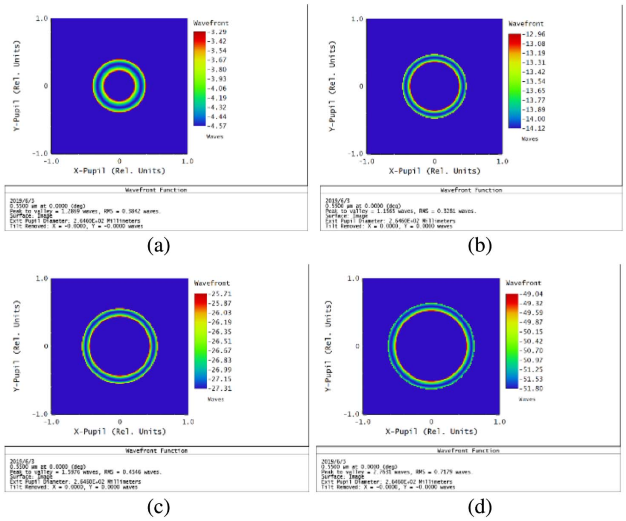

Fig. 8. Positions and departures of tested subapertures. (a) Departure of annular subaperture in the position of 28 to 50 mm in the diameter direction. (b) Departure of annular subaperture in the position of 45 to 60 mm in the diameter direction. (c) Departure of annular subaperture in the position of 55 to 70 mm in the diameter direction. (d) Departure of annular subaperture in the position of 65 to 80 mm in the diameter direction.

The PV and RMS of the original map in the simulation is 0.1513λ and 0.0193λ, respectively. Four tested subapertures are cut from Fig. 9, as shown in Fig. 10.

In actual testing, 6-dof of relative adjustment errors between subapertures will introduce extra aberrations in the testing map. By adding the alignment errors, including piston/tip/tilt to each annular subaperture and considering 2 μm alignment accuracy along the X, Y, and Z directions, respectively, the full-aperture map stitching map can be achieved with our proposed stitching algorithm for annular subapertures. The relative stitching map is shown in Fig. 11.

The PV and RMS of the stitching map is 0.1472λ and 0.0194λ, respectively. Figures 9 and 11 show that the stitching map is consistent with the original map. To better evaluate the

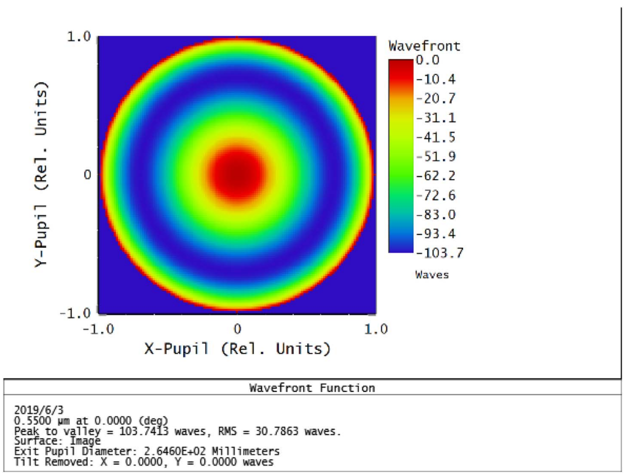

Fig. 7. Departure between aspheric surface and best-fit sphere.

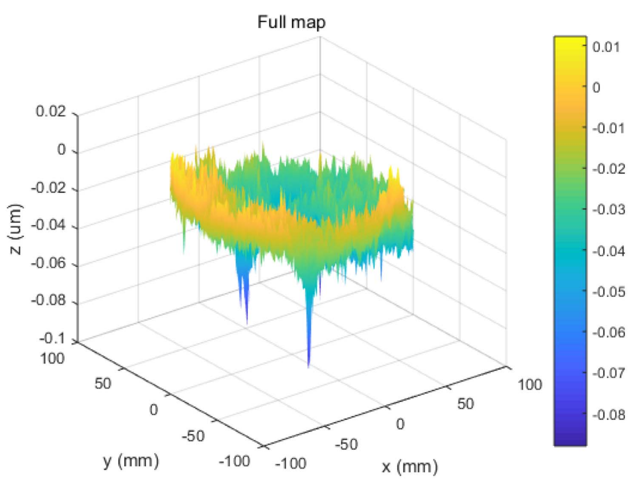

Fig. 9. Original map in the simulation.

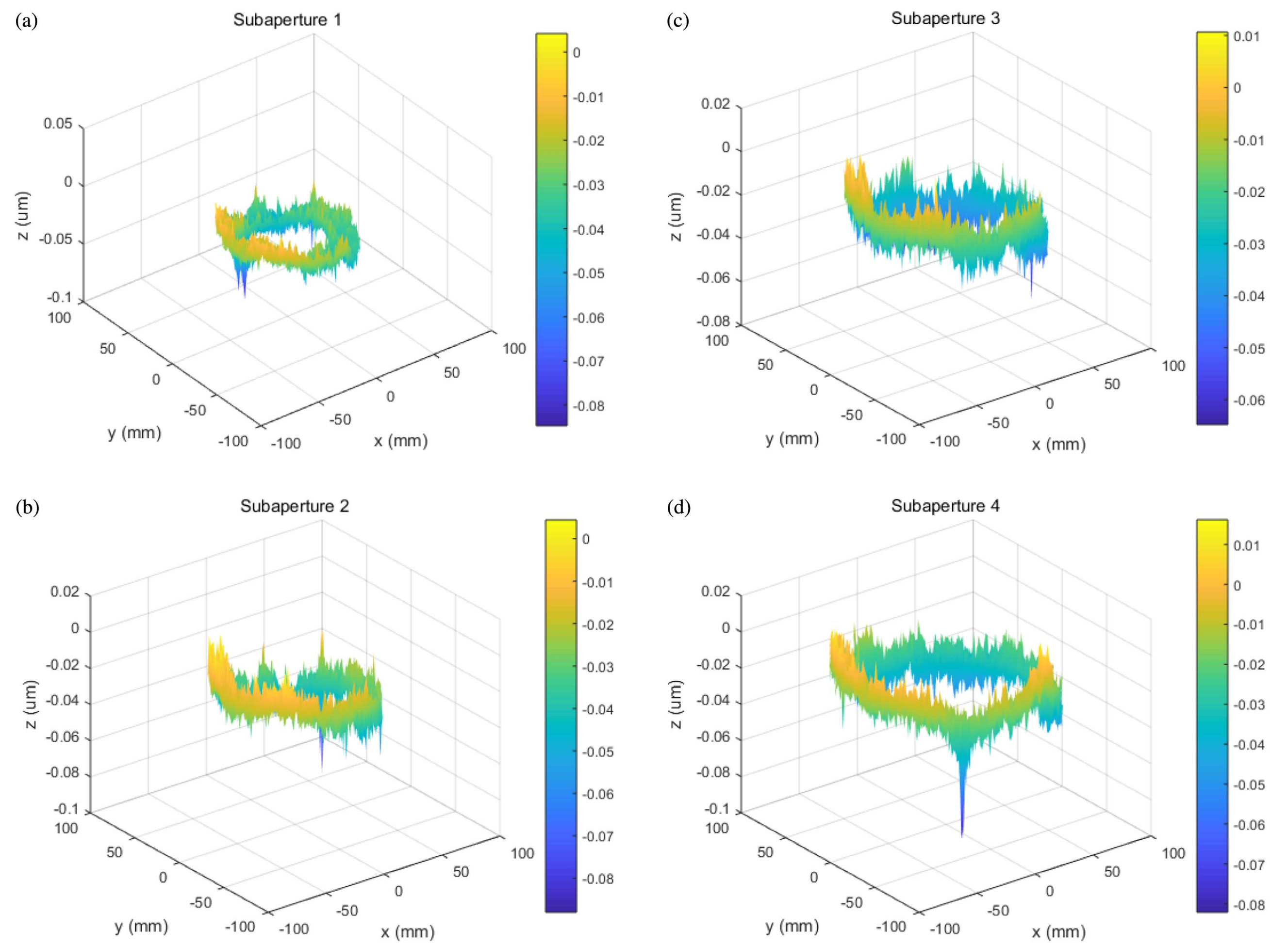

Fig. 10. Tested subapertures: (a) Subaperture 1 (PV 0.138λ, RMS 0.0162); (b) Subaperture 2 (PV 0.143λ, RMS 0.0181); (c) Subaperture 3 (PV 0.113λ, RMS 0.0183); (d) Subaperture 4 (PV 0.146λ, RMS 0.0191λ).

performance of our proposed stitching method, the residual map, which is calculated by subtracting the data between the original full aperture map and the stitching map point by point, is analyzed, as shown in Fig. 12.

It can be seen from Fig. 12 that the PV and RMS of the residual map is 0.0051λ and 0.0011λ ($\lambda = 632.8$ nm), respectively. It is obvious that the original full aperture map matches the stitching map very well, which means the stitching can be

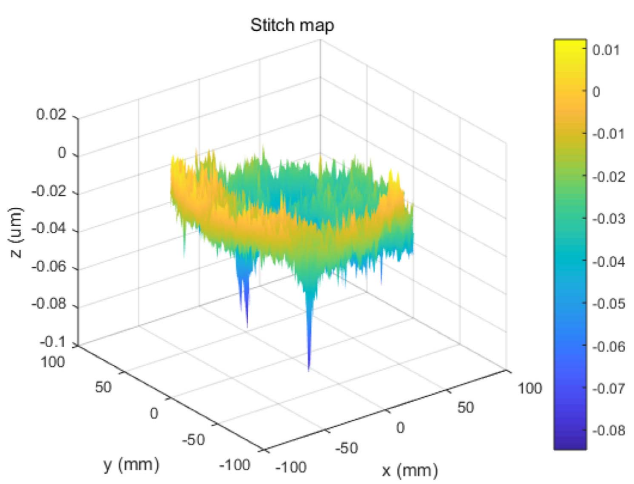

Fig. 11. Stitching map.

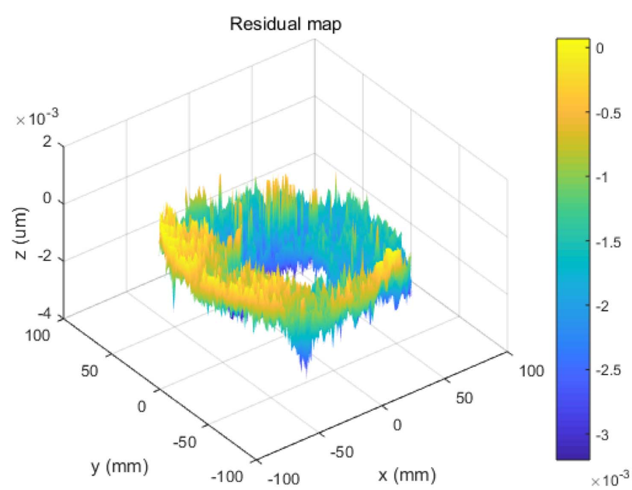

Fig. 12. Residual map.

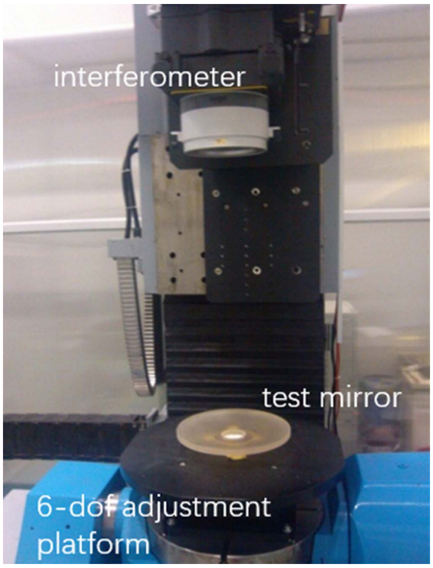

Fig. 13. Experimental setup.

accomplished with our proposed non-null annular subaperture stitching algorithm with satisfactory accuracy.

4. EXPERIMENT

An experiment is carried out to validate the performance of our proposed annular stitching algorithm based on current equipment in the laboratory. In the experiment, a 6-dof platform and a 150 mm interferometer with an $F_{\#}1.1$ standard transmission sphere are applied for the annular subaperture testing, as shown in Fig. 13. The 6-dof platform include the X, Y, Z, A, B, and C axes. The relative relationship between each axis is shown in Fig. 14. The range of movement and relative accuracy of each axis can be found in Table 1. For the rotationally symmetric hyperboloid surface, its internal diameter is 56 mm, while its external diameter is 250 mm. The conic constant k is −1.03, and the vertex radius of the convex mirror is about 513.6 mm.

In the testing, four subapertures are tested, as shown in Fig. 15. For each testing subaperture, the retrace error is included in the testing maps. After removing the retrace error in each subaperture, the full aperture map can be obtained by stitching with our proposed stitching algorithm. The relative stitching map is shown in Fig. 16.

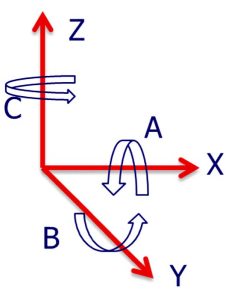

Fig. 14. Description of 6-dof platform.

Table 1. Description of 6-dof Platform

Axis	Range of Movement	Accuracy
X	1000 mm	0.01 mm
Y	500 mm	0.01 mm
Z	800 mm	0.02 mm
A	90°	4″
B	3°	4″
C	360°	10″

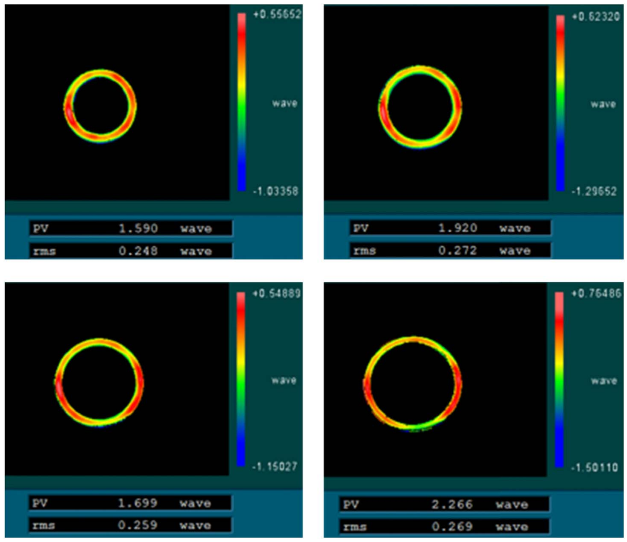

Fig. 15. Four measured annular subapertures.

It can be seen from Fig. 16 that the PV and RMS of the stitching map are 2.135λ and 0.291λ ($\lambda = 632.8$ nm), respectively.

To better evaluate the performance of our proposed stitching algorithm, another subaperture, different from the ones used for stitching, is chosen for stitching accuracy evaluation, as shown in Fig. 17. The residual map between the stitching map and the self-examine subaperture shown in Fig. 17 can be obtained by subtracting the phase data point to point, as shown in Fig. 18.

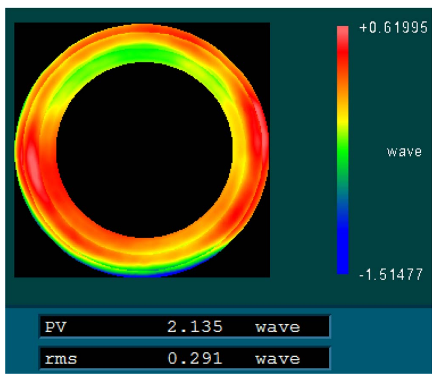

Fig. 16. Stitching map.

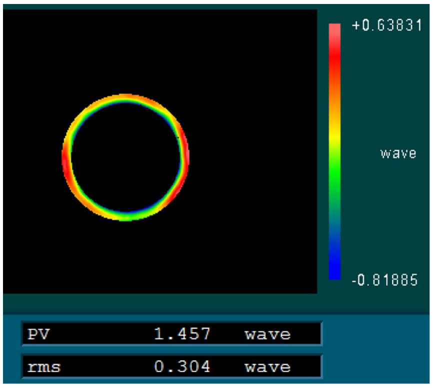

Fig. 17. Subaperture map for accuracy evaluation.

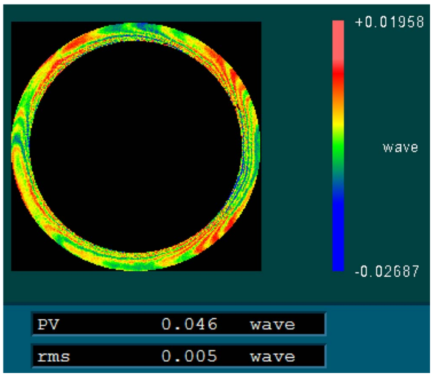

Fig. 18. Residual map.

It is further shown that the PV and RMS errors of the residual map are 0.046λ and 0.005λ, respectively ($\lambda = 632.8$ nm). Considering the alignment accuracy in X, Y, and Z directions in the testing and the environmental effect, the residual is acceptable, and our proposed method is effective for testing rotationally symmetric aspherical surfaces.

5. CONCLUSION

We have proposed an annular subaperture stitching algorithm to test rotationally symmetric aspherical surfaces, which is based on the triangulation interpolation and least-square fitting theory. At the same time, in the non-null stitching, the retrace error in the testing is also analyzed based on the ray tracing method for the central subaperture and annular subaperture, respectively. Simulation is carried out to show that our proposed annular stitching method is effective in the testing for rotationally symmetric aspherical surfaces. To further justify the performance of our stitching method, we tested a rotationally symmetric hyperboloid surface in the experiment, which demonstrated the feasibility of our proposed stitching method. As the experimental stitching testing study is now mainly for mild rotationally symmetric aspherical surfaces, further research is needed for more complex surface forms such as strong aspherical surfaces and free-form surfaces.

Funding. National Natural Science Foundation of China (NSFC) (61805089, 61605202).

REFERENCES

1. S. Peterhänsel, C. Pruss, and W. Osten, “Phase errors in high line density CGH used for aspheric testing: beyond scalar approximation,” Opt. Express **21**, 11638–11651 (2013).
2. T. Ichikawa, T. Yoneyama, and Y. Sakamoto, “CGH calculation with the ray tracing method for the Fourier transform optical system,” Opt. Express **21**, 32019–32031 (2013).
3. Y. He, X. Hou, F. Wu, X. Ma, and R. Liang, “Analysis of spurious diffraction orders of computer-generated hologram in symmetric aspheric metrology,” Opt. Express **25**, 20556–20572 (2017).
4. Y. S. Kim, B. Y. Kim, and Y. W. Lee, “Design of null lenses for testing of elliptical surfaces,” Appl. Opt. **40**, 3215–3219 (2001).
5. S. Xue, S. Chen, Y. Tian, J. Lu, and H. Hu, “Verification and in situ calibration of large-aperture null correctors for convex aspheric mirrors,” Measurement **106**, 79–87 (2017).
6. R. Willstrop, “Null test for a deeply aspheric lens,” Appl. Opt. **50**, 4977–4981 (2011).
7. H. Liu, Z. Lu, F. Li, and Y. Xie, “Full-aperture measurement of convex surfaces in interferometric test using holographic test plates,” Opt. Commun. **241**, 231–236 (2004).
8. C. J. Kim and J. C. Wyant, “Subaperture test of a large flat or a fast aspheric surface,” J. Opt. Soc. Am. **71**, 1587 (1981).
9. J. G. Thunen and O. Y. Kwon, “Full aperture testing with subaperture test optics,” Proc. SPIE **351**, 19–27 (1982).
10. J. E. Negro, “Subaperture optical system testing,” Appl. Opt. **23**, 1921–1930 (1984).
11. S. C. Jensen, W. W. Chow, and G. N. Lawrence, “Subaperture testing approaches: a comparison,” Appl. Opt. **23**, 740–745 (1984).
12. C. R. De Hainaut and A. Erteza, “Numerical processing of dynamic subaperture testing measurements,” Appl. Opt. **25**, 503–509 (1986).
13. S. Y. Chen, S. Y. Li, and Y. F. Dai, “Experimental study on subaperture testing with iterative stitching algorithm,” Opt. Express **16**, 4760–4765 (2008).
14. S. Chen, S. Xue, Y. Dai, and S. Li, “Subaperture stitching test of large steep convex spheres,” Opt. Express **23**, 29047–29058 (2015).
15. Z. Zhao, H. Zhao, F. Gu, H. Du, and K. Li, “Non-null testing for aspheric surfaces using elliptical sub-aperture stitching technique,” Opt. Express **22**, 5512–5520 (2014).
16. L. Zhang, D. Liu, Y. Liu, J. Liu, J. Li, and B. Yu, “Validation of simultaneous reverse optimization reconstruction algorithm in a practical circular subaperture stitching interferometer,” Opt. Commun. **403**, 41–49 (2017).
17. C. Y. Zhao and J. H. Burge, “Stitching of off-axis sub-aperture null measurements of an aspheric surface,” Proc. SPIE **7063**, 706316 (2008).
18. X. Hou, F. Wu, and L. Yang, “Experimental study on measurement of aspheric surface shape with complementary annular subaperture interferometric method,” Opt. Express **15**, 12890–12899 (2007).
19. T. Shi, D. Liu, Y. Zhou, T. Yan, Y. Yang, L. Zhang, J. Bai, Y. Shen, L. Miao, and W. Huang, “Practical retrace error correction in non-null aspheric testing: a comparison,” Opt. Commun. **383**, 378–385 (2017).
20. H. Y. Xu, H. Xian, and Y. D. Zhang, “Comparison of two stitching algorithms for annular subaperture Hartmann Shack testing method,” Proc. SPIE **7849**, 78491Q (2010).
21. Y. F. Wen, H. B. Cheng, and H.-Y. Tam, “Modified stitching algorithm for annular subaperture stitching interferometry for aspheric surfaces,” Appl. Opt. **52**, 5686–5694 (2013).
22. Y. Wen and H. Cheng, “Further investigations of stitching model for annular subaperture interferometric testing based on Zernike annular polynomials,” Optik **126**, 2236–2241 (2015).
23. D. Liu, Y. Yang, C. Tian, Y. Luo, and L. Wang, “Practical methods for retrace error correction in nonnull aspheric testing,” Opt. Express **17**, 7025–7035 (2009).
24. M. Otsubo, K. Okada, and J. Tsujiuchi, “Measurement of large plane surface shapes by connecting small-aperture interferograms,” Opt. Eng. **33**, 608–613 (1994).